International Journal of Thermal Sciences 123 (2018) 140–150

Contents lists available at ScienceDirect

International Journal of Thermal Sciences

journal homepage: www.elsevier.com/locate/ijts

Semi-analytical solutions for the transient temperature fields induced by a moving heat source in an orthogonal domain

T.F. Flint [a, b, *], J.A. Francis [b, *], M.C. Smith [a, b], A.N. Vasileiou [a, b]

[a] Modelling and Simulation Centre, The University of Manchester, Oxford Road, Manchester, UK
[b] School of MACE, The University of Manchester, Oxford Road, Manchester, UK

ARTICLE INFO

Article history:
Received 5 October 2016
Received in revised form
30 June 2017
Accepted 13 September 2017
Available online 4 October 2017

Keywords:
Beam welding
Heat flux model
Heat transfer
Orthogonal geometry
Square-butt weld
Thermal analysis

ABSTRACT

A semi-analytical solution has been derived for the transient temperature fields that are generated in a three-dimensional solid body when it is subjected to one or more moving heat sources. The solution was derived using the Green's function method, and is applicable to any orthogonal domain that is subject to arbitrary boundary conditions. The solution can account for any linear combination of double-ellipsoidal or double-ellipsoidal-conical (DEC) heat sources. It can therefore be applied in situations ranging from an electric arc moving across a flat plate, to partial-penetration or full-penetration welding either with a laser or an electron beam. In this work, full penetration electron beam welds in 30 mm and 130 mm thick sections of SA508 steel were used as experimental test cases. The solution was shown to offer improved accuracy and dramatic reductions in solution times when compared with numerical methods, thereby lending itself to real-time in process monitoring of fusion welding processes.

1. Introduction

The simulation of physical processes in which changes of state occur, with a view to generating predictions for transient temperature fields, is computationally expensive. Advances have been made using fully coupled thermal-fluid simulations using source terms in the Navier-Stokes equations in order to arrest the motion in the solid state [1,2], and source terms in the energy equations to account for latent heat and energy generation [3]. In the modelling of fusion welding processes, another option for the prediction of transient temperature fields is to neglect mass transport associated with weld pool convection and other phenomena, and to solve the heat equation with a representative model of the welding heat source. Three-dimensional volumetric heat sources have been shown to produce the most accurate predictions in such scenarios [4–7]. Nevertheless, both the thermal-fluid solution procedure, and the heat equation solution procedure, are subject to spatial discretisation errors and both rely on closely spaced calculation points in order to predict the evolution of the various fields, particularly the temperature field [8]. Alternatively, semi-analytical techniques may be used [9].

Semi-analytical approaches involve determining the thermal response of a system to an infinitesimally small impulse of heat, and integrating this response over the domain, which is perturbed by the chosen heat source distribution [10,11]. This methodology again neglects any motion in the liquid state and produces a solution to the heat equation. Heat kernels are calculated analytically and then integrated numerically over a desired time interval, which is why such approaches are often referred to as semi-analytical techniques. The most mature of these approaches is the Greens function method [11,12].

A disadvantage associated with semi-analytical methods is that the domain over which the heat kernels are calculated must be orthogonal in order to construct appropriate Dirichlet and/or Neumann boundary conditions using the method of images (MOI). This often limits the application of these heat kernels to idealised scenarios [9]. However, certain physical processes do involve the application of a distributed source of heat to an orthogonal domain, with one example being the electron beam (EB) welding process when applied to the butt-welding of flat plates. Indeed, any fusion welding process, whether it involve an electric arc, a laser or an electron beam, will satisfy these conditions provided that a square-butt weld configuration is employed, regardless of whether the

* Corresponding authors.
E-mail addresses: Thomas.Flint@manchester.ac.uk (T.F. Flint), John.Francis@manchester.ac.uk (J.A. Francis).

https://doi.org/10.1016/j.ijthermalsci.2017.09.012

resulting weld fully penetrates the plates or not. In such cases, the calculation procedure for the heat kernels fundamentally maintains that they are free from discretisation errors, and this is a major advantage of the semi-analytical solution procedure over schemes in which the spatial thermal response is calculated over a discretised grid [13]. Clearly, for either numerical or semi-analytical solution procedures to be representative of a process, an appropriate heat source model must be used [4].

In this work, we present a semi-analytical solution for a welding heat source travelling across an orthogonal domain, and we validate the solution using experimental data that was obtained from the EB welding process. This process utilises a focused beam of high velocity electrons to generate heat at the interface between two mating surfaces. The material in the vicinity of the seam melts and flows together [3]. The high power density causes localised vaporisation, and vapour pressure leads to the formation of a capillary region in the molten weld pool that is often called a keyhole [14]. A keyhole will not form if the power density is insufficient to cause significant vaporisation and, as such, the penetration depth of an incident electron beam into the parent material is related to the beam power density [15]. The prediction of transient temperature fields for the electron beam welding process is of significant interest to the nuclear industry, where models for micro-structural evolution and the development of residual stresses rely on the accurate prediction of welding thermal cycles.

Recently, a heat source model was developed that can represent welding processes in scenarios ranging from an electric arc impinging on a flat plate to an electron beam being applied in the keyhole mode. This model is referred to as the double-ellipsoidal-conical (DEC) heat source model [7]. In this work, the DEC heat source model is incorporated into a Greens function semi-analytical solution procedure and used to predict the transient temperature fields for two EB welding scenarios. Given the inherent flexibility of the DEC heat source model, the solution presented in this work will have numerous applications, and these will not be limited to EB welding. The solution will be applicable to any situation in which an orthogonal domain is subjected to a heat source, or any linear combination of heat sources, where the DEC model can represent each heat source. Furthermore, the computational efficiency associated with this semi-analytical solution may generate opportunities for the application of this approach in real-time process monitoring for high energy density welding processes.

2. Semi-analytical solution procedure

For transient heat conduction, a Green's function can describe the temperature distribution caused by an instantaneous, local heat pulse. The Green's function for a given geometry and set of homogeneous boundary conditions is a building block for the temperature distribution due to a functional initial temperature distribution, and an internal heat flux distribution, q [16]. Multiplication of one-dimensional Green's functions may be used to construct solutions of higher dimensional order [10]. In order to compute the temperature field produced by the DEC heat source model, one must calculate the thermal response due to an infinitesimally small heat quantity, δ, acting instantaneously at time t' and at point (x', y', z') in an infinite domain [9,10]. This response may then be summed with the thermal responses associated with all equivalent heat pulses acting throughout the volume of the domain.

If δ acts instantaneously at time t' and at point (x', y', z') in an infinite domain the infinitesimal rise in temperature due to this point heat pulse $dT_{(x,y,z,t)}$ is given by ${}_{\frac{\delta}{\rho c_p}}K_{(x,x',y,y',z,z',t,t')}dt'$, where K is the three dimensional fundamental solution for an infinite domain, as given by Equation (1) [17]. Here, ρ is the mass density and c_p is the specific heat at constant pressure, $\alpha = {}_{k}/_{\rho c_p}$ is the thermal diffusivity, and k is the thermal conductivity. The temperature increase at a point (x, y, z, t) is then found by integrating from 0 to t.

$$K_{(x,x',y,y',z,z',t,t')} = \left\{ \begin{array}{c} \dfrac{1}{(4\pi\alpha(t-t'))^{3/2}} e^{-\frac{(x-x')^2+(y-y')^2+(z-z')^2}{4\alpha(t-t')}} \quad \forall\ (t-t') \geq 0 \\ 0 \quad \forall\ (t-t') < 0 \end{array} \right\} \tag{1}$$

The MOI may then be used to adapt the solution from one over an infinite domain to one over a finite domain with insulating and Dirichlet boundary conditions, where $\frac{\partial T}{\partial x}$ and T are assigned, respectively, by placing equivalent fictitious sources to absorb or reflect the heat.

Consider an orthogonal domain with dimensions of B, D and L in the x, y and z directions, respectively. Cole et al. [11] demonstrated that the 1D Green's function for insulating boundary conditions ($\partial G/\partial x = 0$, at $x = 0$ and $x = B$) is given by Equation (2), and the 1D Green's function for $\partial G/\partial x = 0$ at $x = 0$ and a Dirichlet boundary condition at $x = B$ is given by Equation (3).

$$G_{(x,x',t,t')} = \sum_{n=-\infty}^{\infty} \frac{e^{-\frac{((2nB)+x-x')^2}{4\alpha(t-t')}} + e^{-\frac{((2nB)+x+x')^2}{4\alpha(t-t')}}}{\sqrt{4\pi\alpha(t-t')}} \tag{2}$$

$$G_{(x,x',t,t')} = \sum_{n=-\infty}^{\infty} (-1^n) \frac{e^{-\frac{((2nB)+x-x')^2}{4\alpha(t-t')}} + e^{-\frac{((2nB)+x+x')^2}{4\alpha(t-t')}}}{\sqrt{4\pi\alpha(t-t')}} \tag{3}$$

For a three dimensional domain with insulating boundary conditions on all faces except a Dirichlet boundary condition on the $x = B$ face the three dimensional Green's function may be found by multiplying the appropriate 1D functions and is shown in Equation (4).

$$G_{(x,x',y,y',z,z',t,t')} = \left\{ \begin{array}{l} (-1^n)\dfrac{e^{-\frac{((2nB)+x-x')^2}{4\alpha(t-t')}} + e^{-\frac{((2nB)+x+x')^2}{4\alpha(t-t')}}}{\sqrt{4\pi\alpha(t-t')}} \times \\ \dfrac{e^{-\frac{((2nD)+y-y')^2}{4\alpha(t-t')}} + e^{-\frac{((2nD)+y+y')^2}{4\alpha(t-t')}}}{\sqrt{4\pi\alpha(t-t')}} \times \\ \dfrac{e^{-\frac{((2nL)+z-z')^2}{4\alpha(t-t')}} + e^{-\frac{((2nL)+z+z')^2}{4\alpha(t-t')}}}{\sqrt{4\pi\alpha(t-t')}} \end{array} \right\} \quad (4)$$

Equation (4) gives the temperature increment at point (x, y, z) and at time t due to an instantaneous unit heat pulse applied at (x', y', z', t'). Due to the linearity of the heat equation, the temperature variation induced at (x, y, z, t) by an instantaneous heat pulse of magnitude $q_{(x',y',z',t')}$ is $\frac{1}{\rho c_p} q_{(x',y',z',t')} G_{(x,x',y,y',z,z',t,t')}$. Assuming that heat has been continuously generated at the point (x', y', z', t') from $t' = 0$, the temperature increment at point (x, y, z, t) is given by Equation (5).

$$(\rho c_p)^{-1} \times \int_0^t q_{(x',y',z',t')} G_{(x,x',y,y',z,z',t,t')} dt' \quad (5)$$

Therefore the temperature increment at any point (x, y, z) and time t due to a distributed heat source $q_{(x',y',z',t')}$ is given by Equation (6).

$$\triangle T(x,y,z,t) = \frac{1}{\rho c_p} \int_0^t \int_0^L \int_0^D \int_0^B q_{(x',y',z',t')} G_{(x,x',y,y',z,z',t,t')} dx' dy' dz' dt' \quad (6)$$

Here, $q_{(x',y',z',t')}$ represents the DEC heat source distribution, which is fully described elsewhere [7]. Surfaces of constant power density in the DEC heat source model are represented schematically in Fig. 1.

In the case of EB welding in keyhole mode, the values of the heat source parameters shown in Fig. 1, in their respective directions, are similar in the double-ellipsoidal and in the conical regions, so that a is similar to a_i, c_r to c_{r_i}, and c_f to c_{f_i}. Consequently, the heat flux distribution takes the form shown in Fig. 2a. It has been shown [7] that more accurate fusion profiles are achieved with a volumetric flux component acting at the surface where the electron beam enters the domain; this volumetric flux accounts for the increased convection at the keyhole surface and is shown in Fig. 2b, where the fraction of power in the surface Gaussian portion of the heat source is f.

In order to solve the heat equation for the double-ellipsoidal-conical heat source, the spatial components of the heat source must be separated. This is equivalent to the conical component of the DEC heat source being independent of the y dimension, so that the double-conical component is treated as a double-cylinder, as shown in Fig. 2a, and the parameters $a = a_i$, $c_r = c_{r_i}$ and $c_f = c_{f_i}$. If the conical quadrants are a function of depth, then the distribution may not be spatially separated, and the spatial integral will not have a closed form analytical solution. In order to compute the transient thermal field due to the double-ellipsoidal-conical flux distribution the following integrals must be performed over the functional components of the DEC distribution.

$$B_T = \sum_{n=-\infty}^{\infty} \int_0^B (-1^n) \frac{e^{-\frac{((2nB)+x-x')^2}{4\alpha(t-t')}} + e^{-\frac{((2nB)+x+x')^2}{4\alpha(t-t')}}}{\sqrt{4\pi\alpha(t-t')}} e^{-3\left(\frac{x'-b_g}{a}\right)^2} dx' \quad (7)$$

$$D_{T_e} = \sum_{n=-\infty}^{\infty} \int_{d_g}^D \frac{e^{-\frac{((2nD)+y-y')^2}{4\alpha(t-t')}} + e^{-\frac{((2nD)+y+y')^2}{4\alpha(t-t')}}}{\sqrt{4\pi\alpha(t-t')}} e^{-3\left(\frac{y'-d_g}{b}\right)^2} dy' \quad (8)$$

$$L_{T_r} = \sum_{n=-\infty}^{\infty} \int_0^{vt'} \frac{e^{-\frac{((2nL)+z-z')^2}{4\alpha(t-t')}} + e^{-\frac{((2nL)+z+z')^2}{4\alpha(t-t')}}}{\sqrt{4\pi\alpha(t-t')}} e^{-3\left(\frac{z'-(vt')}{c_r}\right)^2} dz' \quad (9)$$

$$L_{T_f} = \sum_{n=-\infty}^{\infty} \int_{vt'}^L \frac{e^{-\frac{((2nL)+z-z')^2}{4\alpha(t-t')}} + e^{-\frac{((2nL)+z+z')^2}{4\alpha(t-t')}}}{\sqrt{4\pi\alpha(t-t')}} e^{-3\left(\frac{z'-(vt')}{c_f}\right)^2} dz' \quad (10)$$

The conical portion of the integral that must be computed reduces to

$$D_{T_c} = \sum_{n=-\infty}^{\infty} \int_{y_i}^{d_g} \frac{e^{-\frac{((2nD)+y-y')^2}{4\alpha(t-t')}} + e^{-\frac{((2nD)+y+y')^2}{4\alpha(t-t')}}}{\sqrt{4\pi\alpha(t-t')}} dy' \quad (11)$$

The transient thermal field induced in the finite domain due to the DEC heat source distribution is computed by summing the

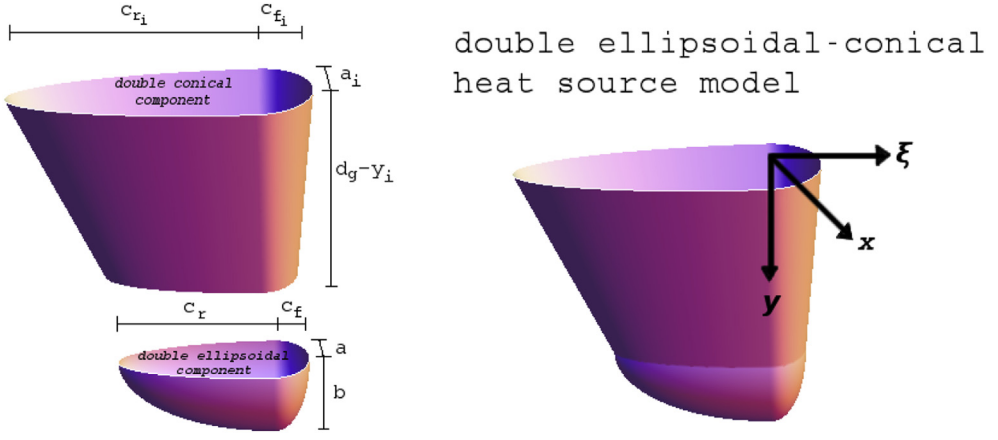

Fig. 1. Schematic diagram of DEC heat source model showing double-ellipsoidal and double-conical regions visualised as surfaces of constant power density.

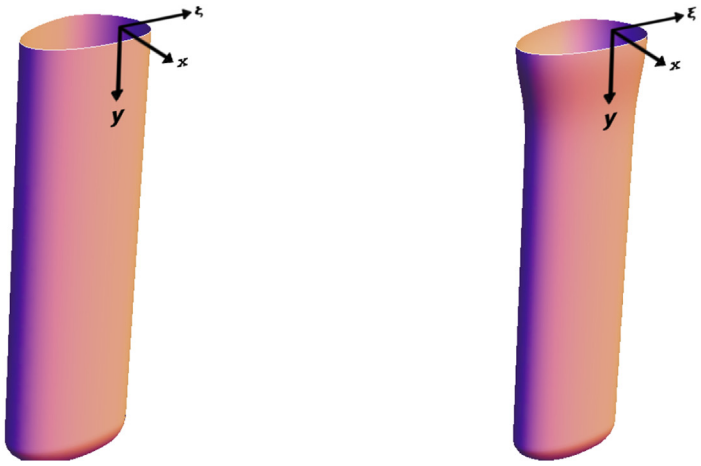

(a) DEC heat source model, showing surfaces of constant power density, used to predict thermal responses in electron beam welding processes without surface Gaussian distribution to model stirring at the surface.

(b) DEC heat source model with 2% heat flux as a surface Gaussian distribution; this addition gives the typical 'nail-head' fusion zone shape in keyhole welding.

Fig. 2. Schematic diagram of the DEC heat source model and representations, 2a without ($f = 0$) and 2b with ($f = 0.02$) the surface Gaussian component, respectively.

contributions from the four quadrants of the DEC heat source according to Equation (12).

$$\Delta T_{DEC(x,y,z,t)} = \frac{1}{\rho c_p}\int_0^t \left\{ \begin{array}{l} \left(Q_{0_{C_r}} B_T D_{T_c} L_{T_r}\right) + \left(Q_{0_{C_f}} B_T D_{T_c} L_{T_f}\right) \\ +\left(Q_{0_{D_r}} B_T D_{T_e} L_{T_r}\right) + \left(Q_{0_{D_f}} B_T D_{T_e} L_{T_f}\right) \end{array} \right\} dt' \tag{12}$$

where $Q_{0_{C_r}} = \frac{54e^3(1-f)R_{r_{conical}}}{\pi^2(e^3-1)S_r(d_g-y_i)}$, $Q_{0_{C_f}} = \frac{54e^3(1-f)R_{f_{conical}}}{\pi^2(e^3-1)S_f(d_g-y_i)}$, $Q_{0_{D_r}} = \frac{6\sqrt{3}(1-f)R_{r_{de}}}{a\ c_r\ b\ \pi\sqrt{\pi}}$ and $Q_{0_{D_f}} = \frac{6\sqrt{3}(1-f)R_{f_{de}}}{a\ c_f\ b\ \pi\sqrt{\pi}}$; the parameters $R_{f_{de}}$, $R_{r_{de}}$, $R_{f_{conical}}$ and $R_{r_{conical}}$ are fully described elsewhere [7]. The thermal contribution from the surface Gaussian distribution is computed according to Equation (13), where a is the radius of the surface Gaussian distribution, and f is the heat fraction apportioned to the surface distribution.

$$\Delta T_{surface(x,y,z,t)} = \frac{f\,6\sqrt{3}\eta VI}{\rho c_p a^3 \pi\sqrt{\pi}}\int_0^t B_T D_{T_e(d_g=0)}\left(L_{T_r(c_r=a)} + L_{T_f(c_f=a)}\right) dt' \tag{13}$$

The temperature increase at any point within the finite domain is then given by the sum of Equation (12) and Equation (13).

3. Performance of analytical solution

Two single pass full penetration EB welds were manufactured in SA508 Grade 3 Class 1 steel, to serve as test cases in assessing the performance of the presented semi-analytical solution for the transient temperature fields in an orthogonal body that is subjected to a DEC heat source. This steel has industrial significance, as it is used to manufacture critical components in the primary circuit of pressurised water reactors, such as the reactor pressure vessel, the steam generators and the pressuriser. Predicted thermal responses, computed using the analytical solution, were compared with measured thermocouple data for experiments performed on 30 mm and 130 mm thick sections. The welded specimens were each instrumented with eight K-type thermocouples, which are effective in measuring temperatures in the range between $-200^{\circ}C$ and $1350^{\circ}C$. The thermocouples were attached in an array that was located at the mid-point along the length of each specimen, such that four sensors were located on the surface where the electron beam was incident and four on the opposite surface, where the electron beam exited the specimen, as shown in Fig. 3a and b for the 30 *mm* and 130 *mm* specimens, respectively. The data sampling rate for the thermocouples was 1 *Hz*.

Equations (12) and (13) were solved and the resulting functions were incorporated into a C++ software program. A double exponential transform algorithm was used for the computation of the final temporal integral. Temperature independent thermal properties were used to represent SA508 steel. The values that were used for the mass density (ρ), the specific heat capacity (c_p) and the thermal conductivity (k) were $7.69 \times 10^{-6}\ kg\ mm^{-3}$, $605\ J\ kg^{-1}\ K^{-1}$ and $0.0334\ W\ mm^{-1}\ K^{-1}$, respectively [18]. In Equations (7) through to (11) the sum from $-\infty$ to ∞ was found to converge rapidly after the $n = 0$ value. For practical applications it was found that the sum $\sum_{n=-10}^{10}$ was sufficient, representing 10 "mirrors" in the MOI approach.

The calibration of a volumetric heat source is best achieved as a two-stage process. Firstly, the overall intensity of the source is calibrated using data from thermocouples that are far enough from the heat source that it can be treated as a point. In such circumstances, the geometry of the heat source has little or no effect on the measured response, positional uncertainty is small and spatter tends not to be a problem. Secondly, the geometry of the heat source is calibrated to match the weld fusion boundary as observed in a transverse weld macrograph. Thermocouples close to the weld pool may also be used to assist in this process, but they are potentially vulnerable to arc shine, spatter, and positional uncertainty associated with attachment in areas of very high spatial temperature gradients. Buried thermocouples may also be used to determine the temperature field within a component during welding. However, reliable thermal contact is difficult to achieve and positional uncertainty is high [19,20]. Calibration of the

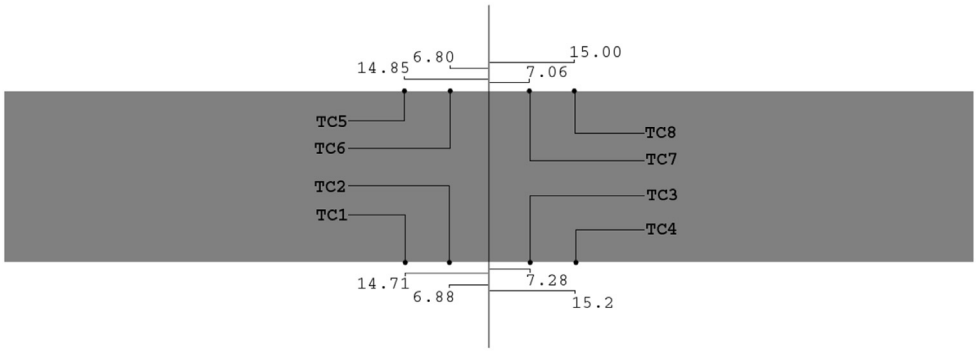

(a) Schematic representation of cross section of 30 mm thick specimen showing measured thermocouple locations.

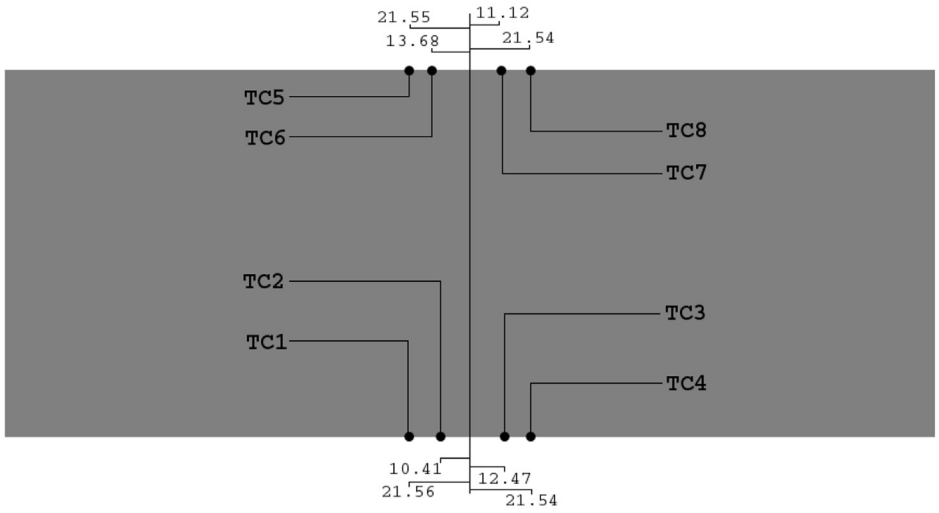

(b) Schematic representation of cross section of 130 mm thick specimen showing measured thermocouple locations.

Fig. 3. Thermocouple locations at the mid-point along the length of the 30 mm thick, *a*, and 130 mm thick, *b*, specimens respectively. All dimensions are in *mm*.

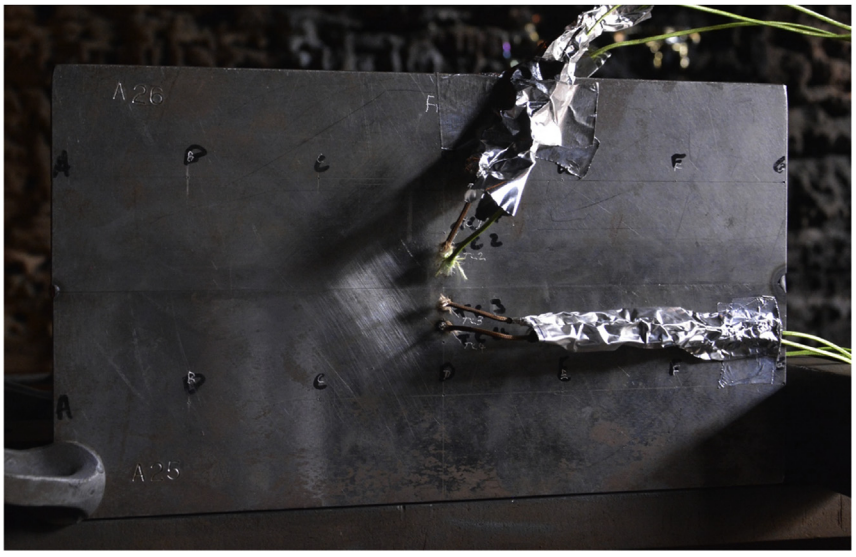

Fig. 4. Experimental set-up for the EB weld before application of the electron beam.

geometric parameters for the heat source (shown in Fig. 1) was carried out using the measured fusion boundary profile as derived from a transverse macrograph, and the transient temperature responses measured in the thermocouples closest to the fusion zone; thermocouples 2, 3, 6 and 7, as shown in Fig. 3 [21,22]. This approach has been used extensively in finite element heat source calibration tools such as FEAT-WMT [19,23]. Electron beam welds are usually excellent candidates for using arrays of thermocouples that are attached at the surface, since narrow fusion zones are produced, and the width of the fusion zone does not vary significantly through the thickness of the weld. If the beam does not deflect under the influence of residual magnetism within the steel, then the responses from the top and bottom surfaces can be expected to be similar, and the differences between the measured peak temperatures at locations close to the fusion zone can be used to determine the geometric parameters of the representative volumetric heat source [24].

3.1. 30 mm thick electron beam weld

The joining of two plates, each 85 *mm* wide, 30 *mm* thick and 300 *mm* long, to form a plate 170 *mm* wide, was performed in a partial vacuum in the 2G position (i.e. with the beam horizontal), as shown in Fig. 4.

The electron beam input current and voltage were 90 *mA* and 150 *kV*, respectively, and the beam traversed along the seam between the two faying surfaces at a velocity of 200 *mm* min^{-1}. The thermocouples were attached at the mid-length position for the weld. Four thermocouples were attached at the $y = 0$ *mm* surface and four at the $y = D$ surface, where in this case $D = 30$ *mm*, as shown in Fig. 3a. The initial temperature of the domain prior to the application of the electron beam was 105 ^oC. Following the joining process the component was left in the vacuum chamber to cool to room temperature.

The parameters y_i, V and I are known from the experiment. The parameter b_g was initially assumed to correspond exactly with the seam between the 85 *mm* wide plates. However, after measurements were carried out on the finished weld, it was found that the beam was actually applied at $x = 84.5$ *mm*. After the efficiency term, η, was found using the "far-field" thermocouples (1, 4, 5 and 8 in Fig. 3a), the parameter f was found by ensuring the correct heat input was observed at thermocouples close to the weld-line on the top and bottom faces. Once the heat fraction in the surface Gaussian component was found there were only 5 unknowns: a, b, c_r, c_f and d_g were required since it can be assumed that $a = a_i$, $c_r = c_{r_i}$ and $c_f = c_{f_i}$. These remaining parameters were found using an iterative process, as detailed above, prior knowledge of the beam diameter, and the knowledge that $d_g + b \geq D$, since the electron beam fully penetrated the work-piece. The heat source parameters used in the analytical simulation of the 30 *mm* thick weld are shown in Table 1, where all units are *mm* unless otherwise stated. Fig. 5 shows the predicted extent of the fusion zone as calculated using the semi-analytical solution procedure. The region bounded by the magenta lines reached temperatures exceeding the solidus temperature for the material, which can be considered to be approximately 1500^oC [24,25].

Table 1
Modelling parameters for the 30 *mm* thick electron beam weld.

Parameter	a	a_i	b	c_r	c_{r_i}	c_f	c_{f_i}	η[a]
Value	1.2	1.2	3.5	4.0	4.0	1.0	1.0	0.58
Parameter	y_i	b_g	v[b]	f[c]	I[d]	V[e]	d_g	b_g
Value	0	85	$3.\dot{3}$	0.02	90	150	28	84.5

[a] Heat transfer efficiency is dimensionless.
[b] Units of velocity are *mm* s^{-1}.
[c] Heat fraction in Gaussian component is dimensionless.
[d] Units of current are *mA*.
[e] Units of voltage are *kV*.

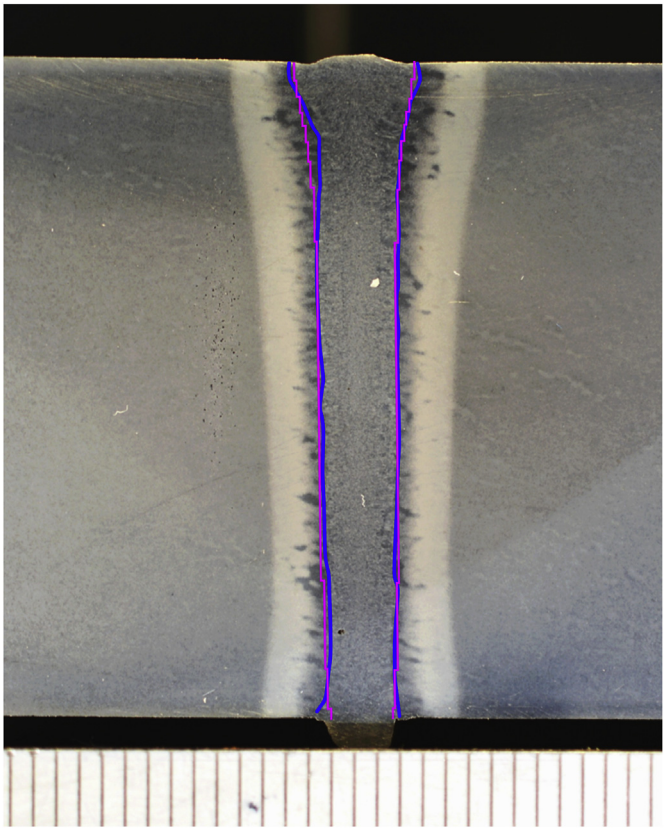

Fig. 5. Comparison of the location of the fusion boundary as observed experimentally (blue lines) and as predicted by the model developed in this work (magenta lines) in the 30 *mm* thick EB weld. (For interpretation of the references to colour in this figure legend, the reader is referred to the web version of this article.)

Comparisons between the thermal cycles recorded by thermocouples and those computed by the analytical solution are shown in Fig. 6.

Fig. 7 shows predicted temperature distributions throughout half of the computational domain, for the 30 *mm* thick specimen, at different times. In all cases, the beam direction is into the page and the top surface of the weld is on the near side. Close examination reveals that the extent of the molten pool is slightly greater near the top of the weld, due to the additional surface heat source component.

The predicted temperatures at the locations corresponding to the thermocouples are in extremely close agreement with the measured temperatures. Particularly notable are the accurate predictions for the temperatures close to the weld-line, where predictions are much more sensitive to the heat source model that is employed. Similarly, the predicted position of the fusion boundary is in close agreement with experimental observations, as shown in Fig. 5. This suggests that both the semi-analytical solution procedure and the DEC heat source model have performed well.

3.2. 130 mm thick electron beam weld

This weld was also manufactured in the 2G welding position. Two plates, each 580 *mm* long, 165 *mm* wide and 130 *mm* thick were joined together to form a welded plate that was 330 *mm* wide.

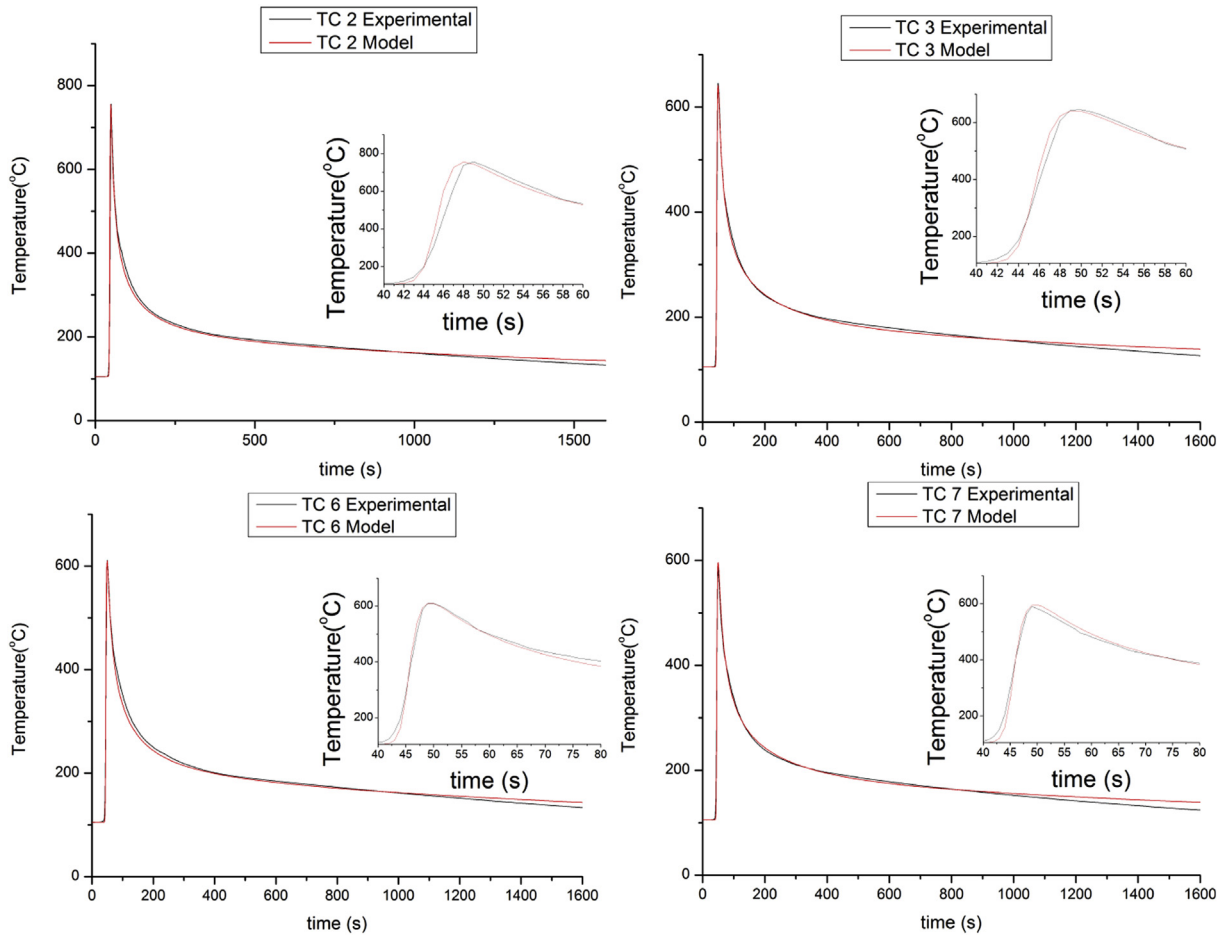

Fig. 6. Comparisons between thermocouple data and predicted thermal responses for the 30 *mm* thick electron beam weld.

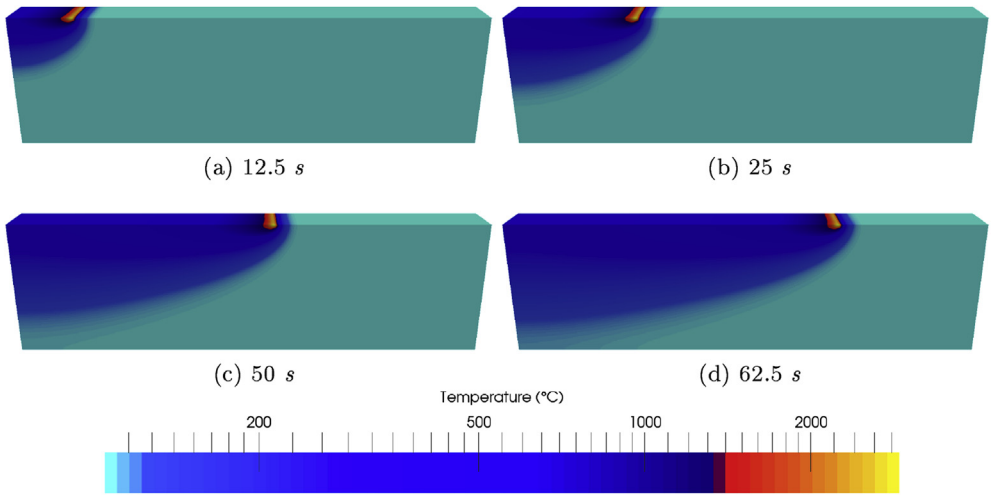

Fig. 7. Plan views showing predicted temperature distributions throughout half of the computational domain, for the 30 *mm* thick specimen at different times. In all cases, the top edge of the domain corresponds to the plane of the weld centreline, and the beam direction is into the page.

Eight thermocouples were attached to the specimen at the mid-length position of the weld. Four thermocouples were attached at the $y = 0$ surface and four at the $y = D$ surface. In this case $D = 130$ *mm*, as shown in Fig. 3b. Again, the work-piece was pre-heated to 105 ^{o}C, and it was allowed to cool to room-temperature in the vacuum chamber following the completion of welding.

Following the same procedure that was employed for the 30 *mm* thick electron beam weld, a Dirichlet boundary condition was applied at the $x = B$ face of the component, since the weld was performed in the 2G position. In the 130 mm thick case, $B = 330$ *mm* and this face was held at $T = 105\ ^{\circ}C$.

In much the same manner as for the 30 mm thick case, the

Table 2
Modelling parameters for the 130 *mm* thick electron beam weld.

Parameter	a	a_i	b	c_r	c_{r_i}	c_f	c_{f_i}	η
Value	1.6	1.6	4	4.5	4.5	0.75	0.75	0.75
Parameter	y_i	b_g	v	f	I	V	d_g	b_g
Value	0	165	1.6̇	0.025	300	150	127	165

fitting parameters were obtained by initially finding the efficiency term, η, using the "far-field" thermocouples (1, 4, 5 and 8 in Fig. 3b), before determining the heat fraction term, f. Then the geometric heat source parameters a, b, c_r, c_f and d_g were found through an iterative process, from knowledge of the beam diameter, and knowing that $d_g + b \geq D$, since this specimen was a full penetration weld. The final heat source parameters that were used in the analytical simulation for the 130 *mm* thick case are shown in Table 2. Fig. 8 shows the predicted position of the fusion boundary as calculated using the semi-analytical solution procedure.

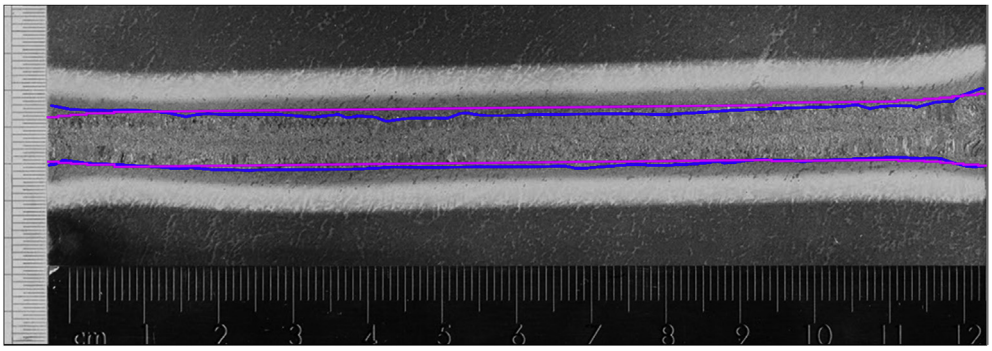

Fig. 8. Location of the fusion boundary in the 130 *mm* thick EB weld according to experimental observations (blue lines) and as predicted by the semi-analytical model (magenta lines). (For interpretation of the references to colour in this figure legend, the reader is referred to the web version of this article.)

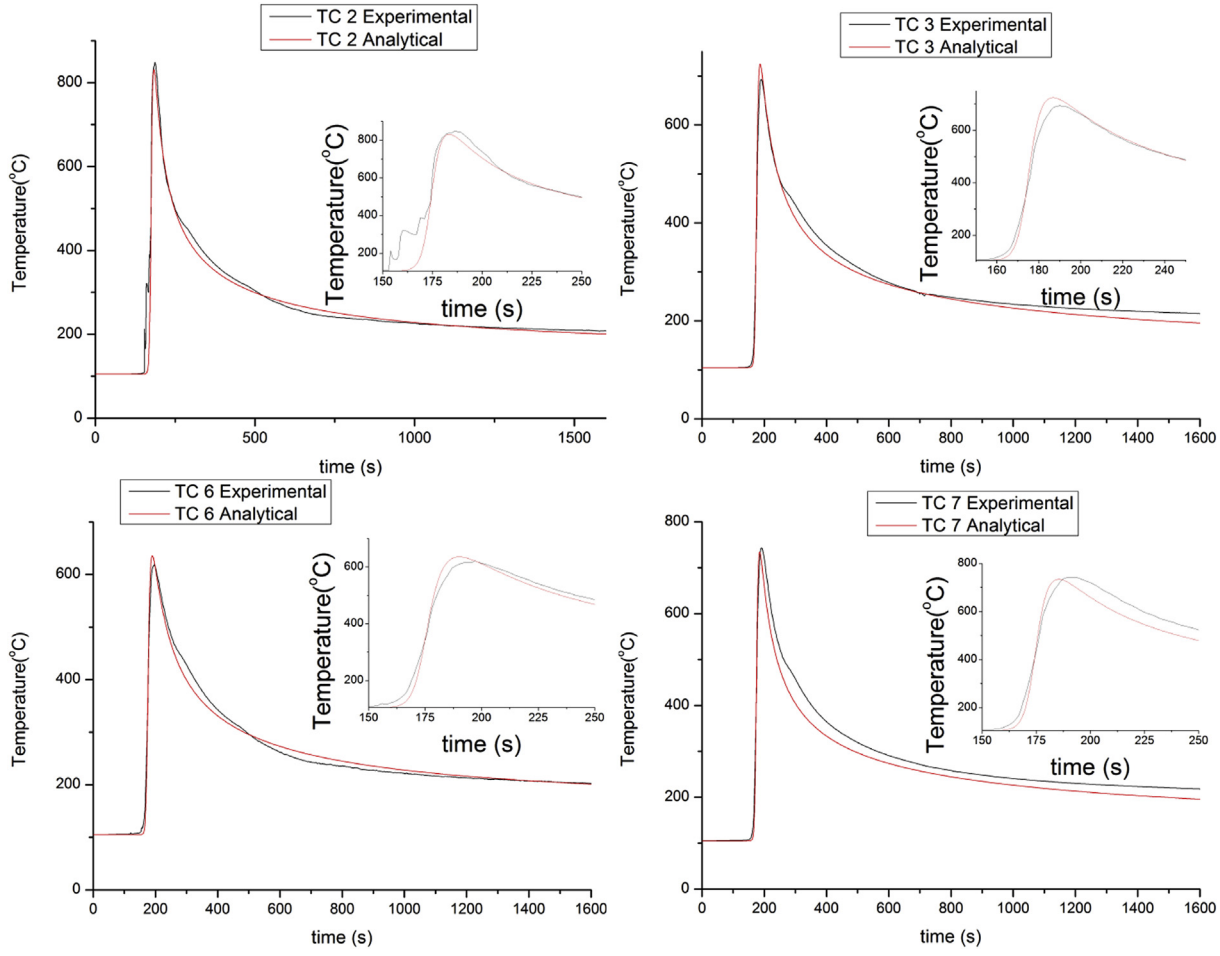

Fig. 9. Comparisons between measured and predicted thermal cycles for the 130 *mm* thick electron beam weld.

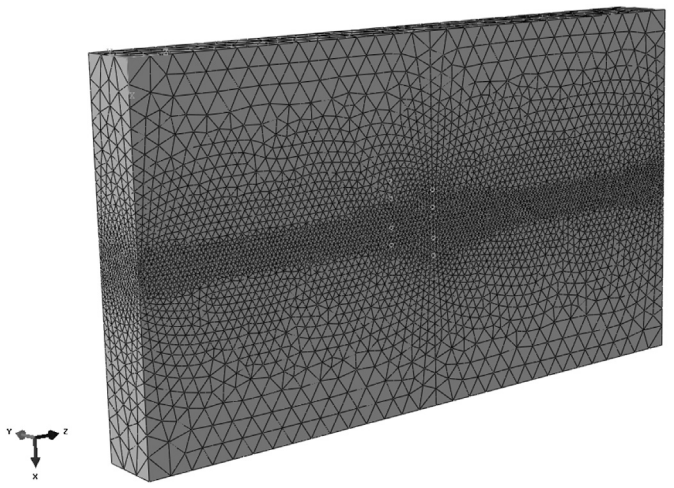

Fig. 10. The FE mesh constructed for the numerical simulation of the 30 mm thick electron beam weld for the purpose of comparison with the analytical solution.

Comparisons between the measured thermal cycles and those predicted using the analytical solution are shown in Fig. 9.

As one might expect, the predicted thermal cycles for the 130 mm thick weld are also in extremely good agreement with those measured experimentally. The predicted peak temperatures close to the fusion zone are in very good agreement with measured values and this again imbues confidence in the DEC heat source model. In general, the accuracy of the temperature predictions for both specimens suggests that the assumption of constant thermal properties did not introduce significant errors. Although the results obtained using the DEC heat source model in combination with the semi-analytical solution procedure were excellent overall, they do not appear to be quite as accurate for the 130 mm thick specimen. There are greater discrepancies between the measured and predicted positions of the fusion boundary, as shown in Fig. 8. The experimentally observed fusion zone exhibits a degree of curvature through the thickness of the weld, and it is noticeably more pronounced than it is for the 30 mm thick case (see Fig. 5). The observed curvature may have been caused by residual magnetism in the welded steel plates, which is a known problem with EB welding. Another possible cause of such curvature is weld pool convection, since buoyancy forces will arise in the weld pool and keyhole when welding in the 2G position. While both of these potential effects are likely to be more prominent in the 130 *mm* thick weld, neither was accounted for in this work.

3.3. Finite element comparison

To demonstrate the computational efficiency of the semi-analytical approach, the predicted temperature fields for the 30 *mm* thick EB weld were compared with those calculated using a finite element (FE) numerical scheme. An FE mesh was constructed, as shown in Fig. 10, and the same DEC heat source with an additional surface component, and the same boundary conditions, were applied. The details of the fitting parameters are given in Table 1. The FE mesh was graded to incorporate more elements around the heat source location, which is necessary to reduce numerical discretisation errors. The FE mesh contained approximately 150,000 10-node quadratic tetrahedral elements.

In Fig. 11 the temperature is plotted as a function of time for three points in the computational domain for both the analytical and the FE analyses. A magnified view of the resulting thermal cycles is also shown in Fig. 11 for the point closest to the path of the heat source.

As one might expect, the analytical and numerical solutions are in almost perfect agreement, since the FE mesh was sufficiently refined in the vicinity of the path of the heat source. The FE simulation was performed on 24 computer nodes, each operating with 5 GB of RAM, and it took approximately 120 h to complete. The analytical solution, running on a single processor, computed the temperature response at the thermocouple locations in approximately two minutes.

When points that are close to the weld centreline (which is located at $x = 84.5\ mm$) are considered, the small discretisation errors in the numerical model become visible. It can be seen from Fig. 11 that the peak temperatures in this region are slightly underestimated in the FE analysis. Fig. 11 shows that further from the weld centreline, the discrepancies between the analytical and the FE predictions are almost non-existent.

In contrast with numerical methods, the nature of the semi-analytical solution ensures that it is not necessary to refine any spatial grids in order to achieve a more accurate solution. If the mesh density in a numerical analysis were to be doubled, the solution time and associated computational costs would scale with this increase in the number of elements. This is not the case for the presented semi-analytical approach, where the temperature history at a given point may be calculated without computing the

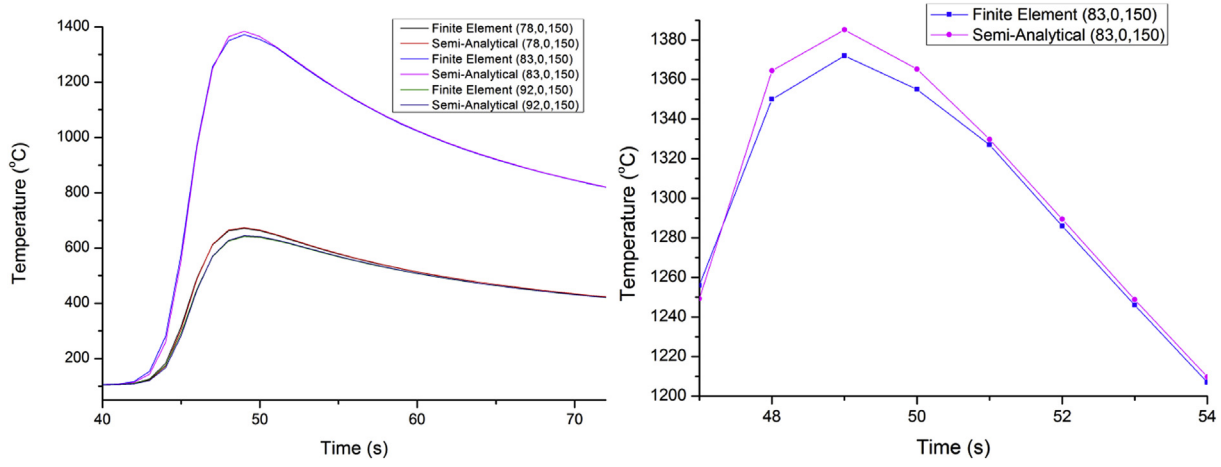

Fig. 11. Comparison between analytically computed temperatures and those computed using the FE method for three points in the 30 *mm* thick electron beam weld.

thermal history for the entire domain. Therefore, if it were necessary to evaluate the temperature at a single point in the vicinity of the EB heat source, this calculation could be performed extremely efficiently using the semi-analytical solution incorporating the DEC heat source model.

4. Discussion

The availability of a representative semi-analytical solution, for the case of a volumetric heat source traversing an orthogonal domain, permits the evaluation of transient temperature fields in a manner that is free of the numerical uncertainties that may arise in numerical methods owing to spatial and temporal discretisation. The predicted temperature fields produced by the semi-analytical approach, when incorporating the DEC heat source model, are clearly representative for the EB welds presented in this work. Extremely good agreement was seen between the predicted and measured transient temperature fields, and also between the predicted and measured locations of the fusion boundary.

The semi-analytical solution, incorporating the DEC heat source, is only suitable for situations in which the domain is orthogonal. However, there are many situations in which square-butt weld preparations are used to join plates, and this solution will be applicable to all such cases, irrespective of whether an electron beam, a laser or an electric arc is used as the heat source. The solution can also accommodate situations in which more than one heat source is applied to the domain, provided that each heat source can be represented by a DEC model. There will be many other processes for which the semi-analytical approach could be used. One such example includes the accurate and rapid calculation of temperature fields in laser-ultrasonics for the purpose of nondestructive evaluation. Dirichlet and Neumann boundary conditions are representative in cases where EB welding is carried out in a vacuum. Green's functions exist which describe film-condition heat loss from a domain, and radiation loss from a domain, so these Green's functions could be used in future work to extend the applicability of the solution.

The accuracy of the predicted temperature fields also provides evidence to suggest that the assumption of constant thermal properties may not introduce significant errors in cases involving SA508 Gr. 3 Cl. 1 steel, at least outside of the fusion zone. The predictions for the 30 mm thick weld were found to be slightly more accurate than those for the 130 mm thick weld. The discrepancies in the thicker weld appeared to be associated with noticeable curvature and asymmetry in the fusion zone. Such curvature is not easy to explain, since the weld would be expected to be nominally symmetric about the weld centreline. One possible explanation for the curvature is that it may be a symptom of residual magnetism within the steel. Since the weld was made in the 2G welding position, weld pool convection and buoyancy effects may also have played some role in introducing this curvature. In future, the application of a thermal-fluid modelling approach may offer further improvements in the predictions for thick-section electron beam welds.

The high computational efficiency achieved with the semi-analytical solution would permit the rapid calculation of transient temperature fields in real-time, as the entire domain need not be solved when using this approach. In contrast, when using numerical techniques, it is necessary to solve the equations explicitly over the entire grid. Unfortunately, a semi-analytical approach of this type cannot be used at present in cases where weld grooves are introduced, or where the components being joined have curvature, since the MOI requires the computational domain to tessellate, and the construction of 3D Green's functions is not possible in these circumstances.

5. Conclusions

For the first time, the semi-analytical solution to the transient heat conduction equation has been computed for the case where a Double-Ellipsoidal-Conical (DEC) heat source distribution with a surface Gaussian component is applied to a finite orthogonal domain with Dirichlet and Neumann boundary conditions. The solution was validated by comparing predicted temperatures with those measured in two electron beam welding experiments, which were performed on 30 mm thick and 130 mm thick sections of SA508 Grade 3 Class 1 steel. Specific conclusions can be drawn as follows:

- Excellent agreement between the predicted and measured temperatures was obtained. The accuracy of the predictions for the peak temperatures on both surfaces of the specimens was particularly notable. This served to validate both the heat flux model as well as the semi-analytical solution technique.
- The solution approach is free of the spatial discretisation errors that are associated with numerical solution procedures.
- A three dimensional Green's function has been constructed that is representative of the EB welding scenarios that were studied in this work. This will prove to be useful for many transient conduction problems and it is not limited to use with the DEC heat source model.
- When using the proposed semi-analytical solution, the computation of the temperature at a given point and at a given time can be carried out independently of the calculation of the temperatures at other points in the computational domain. This is in stark contrast with numerical approaches. As such, the use of this solution is particularly attractive in situations in which the temperature history is only required at certain locations.
- The solution offers the potential to exceed the accuracy that is obtained using numerical analysis techniques in cases where the geometry of the domain is orthogonal.

The principal benefit of the approach is to provide accurate predictions for the temperature at specific points in considerably lower solution times as, when using the proposed method, the heat equation need not be solved over the entire domain to determine the temperature at any given point.

Acknowledgements

The authors wish to acknowledge financial support from the Engineering and Physical Sciences Research Council (EPSRC) through the NNUMAN programme grant in nuclear manufacturing (Grant No. EP/J021172/1).

References

[1] Rösler F, Brüggemann D. Shell-and-tube type latent heat thermal energy storage: numerical analysis and comparison with experiments. Heat Mass Transf 2011;47:1027–33.
[2] Panwisawas C, Qiu CL, Sovani Y, Brooks JW, Attallah MM, Basoalto HC. On the role of thermal fluid dynamics into the evolution of porosity during selective laser melting. Scr Mater. 2015;105:14–7.
[3] Rai R, Burgardt P, Mileewski JO, Lienert TJ, DebRoy T. Heat transfer and fluid flow during electron beam welding of {21Cr-6Ni-9Mn} steel and {Ti-6Al-4V} alloy. J Phys D Appl Phys 2009;42(025503):12.
[4] Goldak JA, Bibby MJ, Chakravarti A. A new finite element model for welding heat sources. Metall Trans B 1984;15:299–305.
[5] Bag S, Trivedi A, De A. Development of a finite element based heat transfer model for conduction mode laser spot welding process using an adaptive volumetric heat source. Int J Therm Sci 2009;48(10):1923–31.
[6] Ghosh Aniruddha, Chattopadhyay Himadri. Mathematical modeling of moving heat source shape for submerged arc welding process. Int J Adv Manuf Technol 2013;69(9–12):2691–701.
[7] Flint TF, Francis JA, Smith MC, Balakrishnan J. Extension of the double-

ellipsoidal heat source model to narrow-groove and keyhole weld configurations. J Mater Process Technol 2017;246:123–35.
[8] Reddy Junuthula Narasimha, Gartling David K. The finite element method in heat transfer and fluid dynamics. third ed. edition. CRC press; 2010.
[9] Fachinotti Victor D, Cardona Alberto, Anca Andres. Analytical solutions of the thermal field induced by moving double-ellipsoidal and double-elliptical heat sources in a semi-infinite body. Numer methods Biomed Eng 2011:595–607.
[10] Fernandes Ana P, Sousa Priscila FB, Borges Valerio L, Guimaraes Gilmar. Use of 3D transient analytical solution based on Greens function to reduce computational time in inverse heat conduction problems. Appl Math Model 2010;34(12):4040–9.
[11] Cole KD, Haji-Sheikh A, Beck James V, Litkouhi Bahman. Heat conduction using Greens functions. 2 edition. Taylor and Francis; 2011.
[12] Flint Thomas F, Francis John A, Yates John R. Analytical solutions of the transient thermal field induced in finite bodies with insulating and convective boundary conditions subjected to a welding heat source. In: Conference proceedings: structural mechanics. Reactor technology, vol. 22; 2013. San Francisco.
[13] Winczek Jerzy. Analytical solution to transient temperature field in a half-infinite body caused by moving volumetric heat source. Int J Heat Mass Transf dec 2010;53(25–26):5774–81.
[14] Geiger M, Leitz K-H, Kock H, Otto A. A 3D transient model of keyhole and melt pool dynamics in laser beam welding applied to the joining of zinc coated sheets. Prod Eng Res Devel 2009;3:127–36.
[15] Roehling Tien T, Wu Sheldon SQ, Khairallah Saad A, Roehling John D, Soezeri S Stefan, Crumb Michael F, et al. Modulating laser intensity profile ellipticity for microstructural control during metal additive manufacturing. Acta Mater 2017;128:197–206.
[16] Wang Baohua, Mazumder Pinaki. Fast thermal analysis for vlsi circuits via semi-analytical green's function in multi-layer materials. In: Circuits and systems, 2004. ISCAS'04. Proceedings of the 2004 international symposium on, vol. 2. IEEE; 2004. II–409.
[17] Carslaw HS, Jaeger JC. Conduction of heat in solids. Oxford University Press; 1959.
[18] Jeyaganesh B, Callaghan MD, Francis JA, English PD, Vasileiou A, Roy MJ, et al. Overview of welding Research under the new nuclear manufacturing (NNUMAN) programme. Mater Fabr 2014;6B:1–8.
[19] Smith MC, Smith AC, Wimpory R, Ohms C. A review of the NeT Task Group 1 residual stress measurement and analysis round robin on a single weld bead-on-plate specimen. Int J Press Vessels Pip 2014;120:93–140.
[20] Smith MC, Smith AC. NeT bead-on-plate round robin: comparison of transient thermal predictions and measurements. Int J Press Vessels Pip 2009;86(1):96–109.
[21] Smith Mike C, Muránsky Ondrej, Austin Colin, Bendeich Philip J, Edwards Lyndon. Optimised modelling of weld metal constitutive behaviour in the NeT TG4 international weld simulation and measurement benchmark. In: ASME 2012 pressure vessels and piping conference. American Society of Mechanical Engineers; 2012. p. 1125–37.
[22] Muránsky Ondrej, Bendeich Philip J, Smith Mike C, Kirstein Oliver, Edwards Lyndon, Holden Tom M. Analysis of residual stresses in three-pass slot weld (NeT-TG4): finite element modelling and neutron diffraction. In: ASME 2010 pressure vessels and piping division/K-PVP conference. American Society of Mechanical Engineers; 2010. p. 1299–305.
[23] Smith RM. FEAT-WMT: weld-modelling tool user guide. FEATWMT: weld-modelling tool user guide. FeatPlus Limited; 2010.
[24] Vasileiou Anastasia N, Smith Michael C, Balakrishnan Jeyaganesh, Francis John A, Hamelin Cory J. The impact of transformation plasticity on the electron beam welding of thick-section ferritic steel components. Nucl Eng Des 2017;323:309–16. https://doi.org/10.1016/j.nucengdes.2017.03.040. ISSN 0029-5493, http://www.sciencedirect.com/science/article/pii/S0029549317301607.
[25] Francis JA, Bhadeshia HKDH, Withers PJ. Welding residual stresses in ferritic power plant steels. Mater Sci Technol 2007;23(9):1009–20.